Center for Turbulence Research
Proceedings of the Summer Program 2008

Modeling full-Mach-range cavitating flow with sharp interface model

By X. Y. Hu†, N. A. Adams†, E. Johnsen AND G. Iaccarino

In this work, two extensiosn of our previous work are proposed for the simulation of full-Mach-range cavitating flow with sharp interface model. These extensions are: a new interface-interaction solver, which includes a new HLLC Riemann solver suitable for both strong and weak interface interaction with general EOS, and a simple phase-change model which assumes that the phase change is in thermal non-equilibrium, and is much slower than the interaction described by the Riemann problem. Several numerical examples in one dimension are studied; the results suggest that the present method exhibits good robustness and accuracy.

1. Introduction

Cavitating flow is still difficult for modern computational fluid dynamics. Generally, the difficulty is strongly related with the numerical methods for the material interface. First, the numerical method should be able to resolve the interface accurately and solve the interface interaction between the heavy and stiff liquid medium and the light and soft gaseous medium. Second, the numerical method should be able to treat the interface interaction between different Mach-number regions. Specifically, the flow in the liquid region is usually a low-Mach-number flow because the liquid is only weakly compressible, but the flow on the other side of the interface, i.e., in the air or vapor region, is typically transonic since the gaseous medium is compressible, especially during the bubble collapse. Furthermore, when the homogeneous model for the vapor/air/liquid mixture is used, the associated flow is typically supersonic because of the highly compressible property of the mixture. Third, the numerical method should be able to take into account the mass, momentum and energy exchange at the interface associated with phase-change phenomena, such as evaporation and condensation. Finally, the numerical method should be able to handle nucleation, in which new material interface is created in liquid bulk.

Recently, we presented a conservative interface method for both multi-fluid and complex boundary problems, in which the standard finite-volume scheme on Cartesian grid is modified by considering computational cells being cut by the interface. While the discretized governing equations are updated conservatively, the method solves the difficulty of conservation for the front-tracking method and treats topological change naturally by combining the interface description and geometric operations with a level-set technique. As the interface condition is obtained by solving the Riemann problem, it is capable of solving shock interface interactions stably and accurately. This method has been successfully used for interfacial flows including liquid/gas interaction (Hu *et al.* 2006). However, in order to simulate cavitating flow, there are still several important issues to be addressed for the interface-interaction solver. First, for accuracy and robustness, an iterative two-rarefaction-wave approximate Riemann solver is used. To avoid the

† Lehrstuhl für Aerodynamik, Technische Universität München, Germany

difficulties of no-convergence and multiple solutions, the iterative root-finding algorithm may become quite complicated and require more computational overhead, especially for fluids with general equation of state (EOS). Second, while the current Riemann solver is accurate and robust for strong interaction with shock, it, just like other approximate Riemann solvers, has difficulty with weak interaction (low-Mach-number problems) when the interface velocity is small compared to the sound speed (Guillard & Murrone 2004). Furthermore, the interface-interaction solver has not extended for phase-change and nucleation phenomena.

Here, we propose two extensions of our previous work on the simulation of full-Mach-range cavitating flow with sharp interface model. Specifically, we provide a new interface-interaction solver, which solves the Riemann problem in a non-iterative, one-step fashion, is suitable for both strong and weak interface interaction with general EOS, and takes into account the effects of phase-change phenomena such as evaporation and condensation.

2. Method

Assuming the fluid is inviscid and compressible, the governing equation of the flow can be written as a system of conservation laws:

$$\frac{\partial \mathbf{U}}{\partial t} + \nabla \cdot \mathbf{F} = 0 \quad \text{on } \Omega, \tag{2.1}$$

where $\mathbf{U}$ is the density of the conserved quantities of mass, momentum and total energy, and $\mathbf{F}$ represents the corresponding flux functions. When a material interface $\mathcal{I}(t)$ separates the domain Ω into two parts, the fluid states in the left and the right sub-domains $\Omega_l(t)$ and $\Omega_r(t)$ are described by different EOS. If no phase change is considered, the evolution of the interface, and the exchange of the momentum and energy for hydrodynamic interaction across the interface, are determined by solving a 1-D, two-material Riemann problem,

$$\mathcal{R}(\mathbf{U}_l, \mathbf{U}_r) = 0 \quad \text{on } \mathcal{I}(t), \tag{2.2}$$

where $\mathbf{U}_l$ and $\mathbf{U}_r$ represent the left and right states in the normal direction (Hu *et al.* 2006). Neglecting the contribution in the tangential direction, the 1-D governing equation in the normal direction can be written in the form as

$$\mathbf{U}_t + \mathbf{F}(\mathbf{U})_x = 0, \tag{2.3}$$

where $\mathbf{U} = (\rho, \rho q, E)^T$ and $\mathbf{F}(\mathbf{U}) = (\rho u, p + \rho q^2, u(E+p))^T$ together with $E = \rho e + \frac{1}{2}\rho q^2$, where ρ, p and e represent the density, pressure and specific internal energy, respectively, and q and E represent the velocity normal to the interface and the total energy, respectively. We assume a general EOS with the form

$$p(\rho, e) = \Gamma(\rho)\rho e + f(\rho) \tag{2.4}$$

in which Γ is the Grüneisen coefficient. Equation (2.4) generalizes an adequate approximation to a wide variety of materials of interest. This includes materials such as ideal gases, stiff gases, explosives and condensed materials under high pressure. Note that there are usually different expressions of $p(\rho, e)$ across the interface. The sound speed c is given by

$$c^2 = \frac{\partial p}{\partial \rho}|_e + \frac{p}{\rho^2}\frac{\partial p}{\partial e}|_\rho = \Psi + \Gamma\frac{p}{\rho}. \tag{2.5}$$

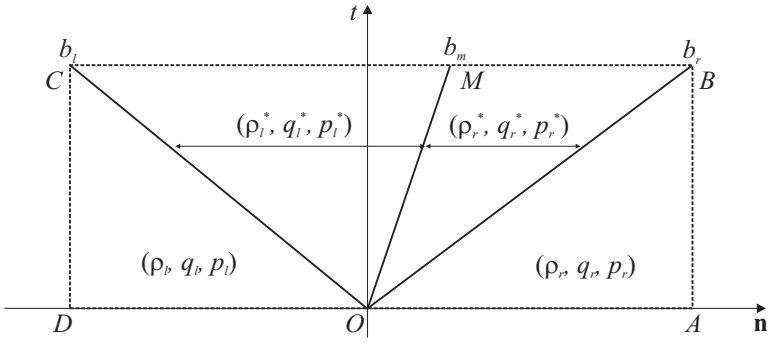

FIGURE 1. Simplified Riemann fan with two intermediate states.

2.1. *A new HLLC solver*

The Harten, Lax, and van Leer with contact restoration (HLLC) Riemann problem (Harten *et al.* 1983; Toro *et al.* 1994) approximates the Riemann fan, as shown in Fig. 1, with two waves having the smallest and largest velocity, denoted as b_l and b_l, respectively, and a middle or contact wave whose speed is denoted as b_l. There are two average intermediate states, (ρ_l^*, q_l^*, p_l^*), (ρ_r^*, q_r^*, p_r^*), separated by the contact wave denoted as b_m. By assuming that the contact wave and intermediate state has relation $b_m = q_l^* = q_r^* = q^*$ and $p_l^* = p_r^* = p^*$, the integration of equation (2.3) over the time-space rectangle $ABCD$, as shown in Fig. 1, gives

$$\rho_r b_r - \rho_l b_l + \rho_l q_l - \rho_r q_r = \rho_l^*(q^* - b_l) + \rho_r^*(b_r - q^*) \tag{2.6}$$

$$\rho_r q_r(b_r - q_r) + \rho_l q_l(q_l - b_l) + p_l - p_r = \rho_l^* q_l^*(q^* - b_l) + \rho_r^* q_r^*(b_r - q^*) \tag{2.7}$$

$$E_r b_r - E_l b_l + (E_l + p_l)q_l - (E_r + p_r)q_r = E_l^*(q^* - b_l) + E_r^*(b_r - q^*). \tag{2.8}$$

Application of Eqs. (2.6) and (2.7) results in

$$q^* = \frac{\rho_r q_r(b_r - q_r) + \rho_l q_l(q_l - b_l) + p_l - p_r}{\rho_r(b_r - q_r) + \rho_l(q_l - b_l)}. \tag{2.9}$$

Note that Eq. (2.9) has the same form as that obtained by Toro *et al.* (1994). Since there is no flux of mass across the contact wave, as shown in Fig. 1, the integrations of density over the time-space region $OMCD$ and $OABM$ gives the intermediate densities

$$\rho_l^* = \rho_l \frac{b_l - q_l}{q^* - b_l}, \quad \rho_r^* = \rho_r \frac{q_r - b_r}{b_r - q^*}. \tag{2.10}$$

Other than using the jump relations (two-shock approximation) as in Toro *et al.* (1994), the present solver obtains the interface pressure by solving Eq. (2.8) with the EOSs given by Eq. (2.4). The result is

$$p^* = \frac{\Gamma_l(\rho_l^*)\Gamma_r(\rho_r^*)}{\beta\Gamma_l(\rho_l^*) + \alpha\Gamma_r(\rho_r^*)} \left[(\rho e)^* + \left(\alpha \frac{f_l(\rho_l^*)}{\Gamma_l(\rho_l^*)} + \beta \frac{f_r(\rho_r^*)}{\Gamma_r(\rho_r^*)}\right)\right] \tag{2.11}$$

where

$$\alpha = \frac{q^* - b_l}{b_r - b_l}, \quad \beta = \frac{b_r - q^*}{b_r - b_l}, \quad \alpha + \beta = 1,$$

$$(\rho e)^* = \frac{1}{b_r - b_l}\left[E_r b_r - E_l b_l + (E_l + p_l)q_l - (E_r + p_r)q_r\right] - \frac{1}{2}\left(\alpha\rho_l^* + \beta\rho_r^*\right) q^{*2}.$$

At the weak interaction (or low-Mach number) limit, one has the approximations $q_l - b_l \approx q^* - b_l \approx c_l \gg |q_l|$, $b_r - q_r \approx b_r - q^* \approx c_r \gg |q_r|$ and $\max(|q_{n,l}|, |q_r|) \ll \min(c_l, c_r)$. From Eq. (2.11), one can easily find the interface pressure at the low-Mach number limit is

$$p^*_{M_*} = \frac{\Gamma_l(\rho^*_l)\Gamma_r(\rho^*_r)}{\beta\Gamma_l(\rho^*_l) + \alpha\Gamma_r(\rho^*_r)}\,(p_l + p_r)\,, \tag{2.12}$$

in which the acoustic pressure wave vanishes. For the HLLC solver of Toro *et al.* (1994), the interface pressure is given by

$$p^* = \rho_l(q_l - b_l)(q_l - q^*) + p_l. \tag{2.13}$$

At the weak interaction (or low-Mach number) limit, the interface pressure given by Eq. (2.13) is

$$p^*_{M_*} = \rho_l c_l(q_l - q^*) + p_l. \tag{2.14}$$

Equation (2.14), like several other linearized Riemann solvers, is the same as the first-order approximation of accurate Riemann solver (Guillard & Murrone 2004), which suggests that even if the initial data are close to a constant density incompressible field, the field computed by Eq. (2.13) contains, after one time step, acoustic pressure waves that are much larger than the pressure fluctuations due to the weak interaction. This is not physical and may introduce numerical instability.

In this paper, the HLLC solver is proposed to solve the two-material Riemann problem given by Eq. (2.2), i.e., the interface condition is obtained by the contact wave velocity u^* with Eq. (2.9) and the intermediate pressure p^* with Eq. (2.11). With the interface condition, according to Hu *et al.* (2006), the rates of momentum and energy exchanges at interface without phase change can be obtained by

$$\hat{\mathbf{X}}^{\mathbf{P}}(\Delta\mathcal{I}) = p^*\Delta\mathcal{I}\mathbf{N}_I, \quad \hat{X}^E(\Delta\mathcal{I}) = p^*q^*\Delta\mathcal{I}, \tag{2.15}$$

where $\mathbf{N}_I$ is the normal direction of the interface and $\Delta\mathcal{I}$ is the interface area patch in a computational cell.

It is suggested that the wave speeds, b_l and b_r, be estimate by

$$b_l = \min[u_l - c_l, \tilde{q} - \tilde{c}], \quad b_r = \max[\tilde{q} + \tilde{c}, u_r + c_r], \tag{2.16}$$

where c is the sound speed, and the tilde $\tilde{}$ represents the Roe-averaged values (Einfeldt *et al.* 1991, Batten *et al.* 1997). For the two-fluid problem with general EOSs, the Roe-averaged sound speed and velocity is obtained by a generalized formulation (Hu *et al.* 2008):

$$\tilde{\rho} = \sqrt{\rho_l\rho_r}, \quad \tilde{g} = \mu(g) = \frac{\sqrt{\rho_l}g_l + \sqrt{\rho_r}g_r}{\sqrt{\rho_l} + \sqrt{\rho_r}}, \quad g = q, \Gamma, \Psi \tag{2.17}$$

and

$$\tilde{c}^2 = \tilde{\Psi} + \tilde{\Gamma}\widetilde{\left(\frac{p}{\rho}\right)} \tag{2.18}$$

with

$$\widetilde{\left(\frac{p}{\rho}\right)} = \mu\left(\frac{p}{\rho}\right) + \frac{1}{2}\tilde{\rho}\left(\frac{q_r - q_l}{\sqrt{\rho_l} + \sqrt{\rho_r}}\right)^2.$$

2.2. *Phase-change model*

To model the phase change at the interface, we apply the thermal non-equilibrium assumption (Fujikawa & Akamatsu 1980), by which, during the phase-change process, while

the pressure is equilibrium at the vapor pressure, the temperature has a discontinuity at the phase interface. The expression for the rate of evaporation and condensation $\dot{m}$ has the form (Schrage 1953):

$$\dot{m} = \frac{\alpha}{\sqrt{2\pi R_v}} \left(\frac{p_s(T_{li})}{\sqrt{T_{li}}} - \frac{p_v}{\sqrt{T_v}} \right). \tag{2.19}$$

Here, α is the accommodation coefficient for evaporation or condensation (assumed constant), equal to the ratio of vapor molecules sticking to the phase interface to those impinging on it; T_v and T_{li} are the temperatures of the vapor and the liquid at the phase interface, respectively; R_v is the gas constant of the vapor; p_v is the actual vapor pressure at the phase interface, and $p_s(T_{li})$ is the equilibrium (saturation) vapor pressure at temperature T_{li} and is obtained from the Clausius-Clapeyron equation

$$p_s(T_{li}) = p_0 \exp\left[\frac{L_v}{R_v} \left(\frac{1}{T_0} - \frac{1}{T_{li}} \right) \right], \tag{2.20}$$

where L_v is the latent heat of vaporization, and p_0 and T_0 are given by a reference saturation state. With Eq. (2.19), the phase-change-induced interface velocity is

$$\Delta q^* = \frac{\dot{m}}{\rho_{li}}, \tag{2.21}$$

where ρ_{li} is the density of liquid at the phase interface. In a cavitating flow, Δq^* usually is small and much smaller than the advection velocity of the interface (Brennen 1995), which suggests that the change rates of pressure and temperature caused by the latent heat are insignificant. Therefore, it is straightforward to assume that the phase change is much slower than the hydrodynamic interface interaction. If the effects of heat conduction in the bulk are also neglected, one can simply obtain p_v, ρ_{li}, T_{li} and T_v from the previous interface-interaction solver

$$p_v = p^*, \quad \rho_{li} = \rho_{li}^*, \quad T_{li} = T(p^*, \rho_{li}^*), \quad T_v = T(p^*, \rho_v^*), \tag{2.22}$$

in which the superscript * represents intermediate states in Eqs. (2.10) and (2.11).

Similar to Eq. (2.15), the rates of mass, momentum and energy exchanges at the interface associated with phase change can be obtained by

$$\hat{\mathbf{X}}^m(\Delta\mathcal{I}) = \dot{m}\Delta\mathcal{I}, \quad \hat{\mathbf{X}}^{\mathbf{P}'}(\Delta\mathcal{I}) = \dot{m}[\mathbf{v}^*]\Delta\mathcal{I}, \quad \hat{X}^{E'}(\Delta\mathcal{I}) = (\dot{m}[E^*] + p^*\Delta q^*)\Delta\mathcal{I}, \tag{2.23}$$

where $[\cdot]$ gives the interfacial state which is chosen from the liquid for evaporation and the vapor for condensation. Note that the energy exchange usually is not important for water because the introduced temperature change is negligible.

3. Numerical examples

The following 1-D numerical examples are provided to illustrate the potential of the present HLLC solver. For all test cases, we use a conservative interface method for multi-fluid problems (Hu *et al.* 2006) in which one-phase calculations are carried out with a fifth-order WENO-LLF (Jiang & Shu 1996) and a third-order TVD Runge-Kutta scheme (Shu & Osher 1988). To decrease the over-dissipation in smooth regions caused by the WENO limiter, a technique of Borges *et al.* (2008) is used. We shall denote "TR" for results obtained by the two-rarefaction-wave Riemann solver (Hu & Khoo 2004), "HLLC" by the original HLLC solver, and "M-HLLC" by the present HLLC solver. The number

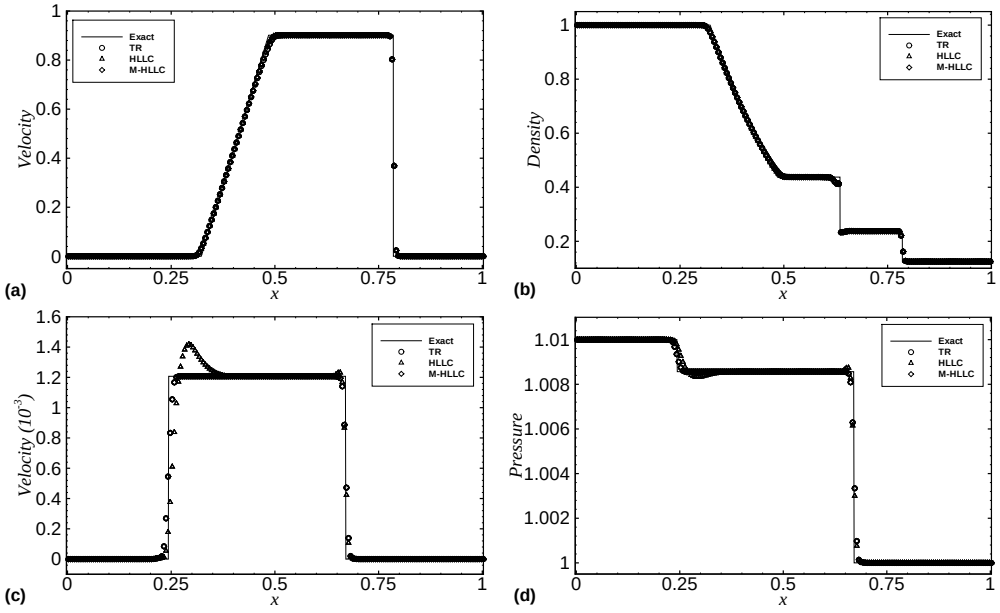

FIGURE 2. Shock tube problems: Case I-A (a) and (b); Case I-B (c) and (d).

of grid points is 200 and the referenced exact solution, if given, is sampled on 1000 grid points. All the computations are carried out with the CFL number of 0.6.

3.1. *Shock tube problems (I)*

Nest we consider two shock tube problems of two gases modeled by ideal gas EOS, $p = (\gamma - 1)\rho e$, where γ is constant, with very different shock strengths. For Case I-A, which is taken from Fedkiw *et al.* (1999), Hu & Khoo (2004) and Hu *et al.* (2006), the shock is moderately strong. The initial conditions are

$$(\rho, u, p, \gamma) = \begin{cases} (1, 0, 1, 1.4) & \text{if } 0 < x < 0.5 \\ \\ (0.125, 0, 0.1, 1.667) & \text{if } 1 > x > 0.5 \end{cases}. \tag{3.1}$$

and the final time is $t = 0.15$. For Case I-B, the initial conditions are

$$(\rho, u, p, \gamma) = \begin{cases} (1, 0, 1.001, 1.4) & \text{if } 0 < x < 0.6 \\ \\ (30, 0, 1.0, 1.667) & \text{if } 1 > x > 0.6 \end{cases} \tag{3.2}$$

in which the shock is weak but there is large density ratio at the interface. The final time is $t = 0.3$.

Figure 2 gives the computed velocity, density or pressure profiles. There are good agreements with exact solutions, except that, for Case I-B, the original HLLC solver predicts much larger errors than the two-rarefaction approximation solver and the present HLLC solver.

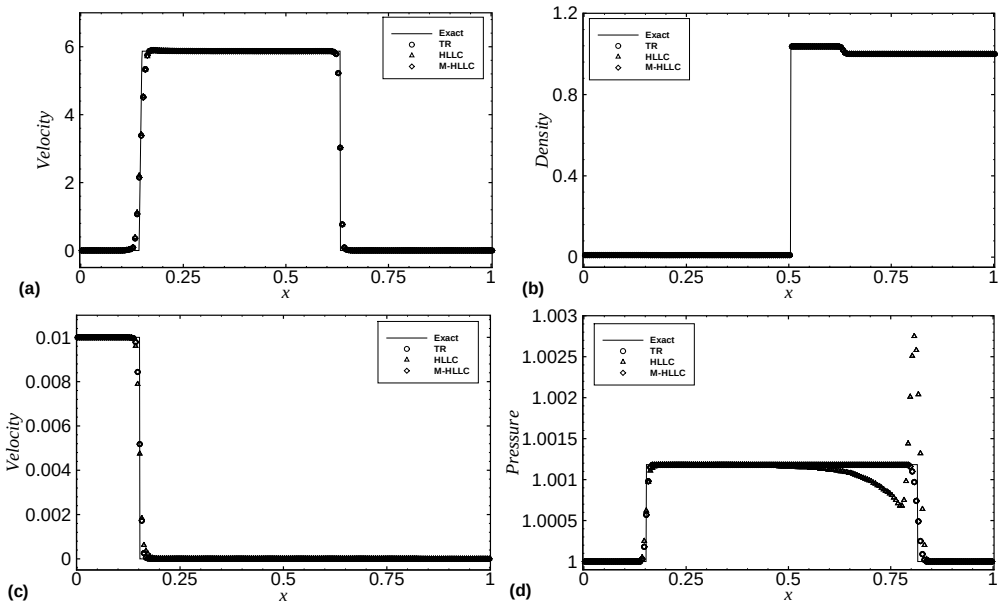

FIGURE 3. Interaction with water: Case II-A (a) and (b); Case II-B (c) and (d).

3.2. *Interaction with water (II)*

We consider two problems with gas-water interaction, in which the gas is modeled with ideal-gas EOS and water is modeled with Tait's EOS, $p = B\left(\frac{\rho}{\rho_0}\right)^{\gamma} - B + A$, where $\gamma = 7.15$ and the non-dimensional parameters are $B = 3310$, $A = 1$ and $\rho_0 = 1$ with respect to the property of water at 1 atmosphere and length scale 1 m. For Case II-A, which is taken from Hu & Khoo (2004), the high-pressure gas expands slowly compared to the transmitted and reflected wavefront speeds. The initial conditions are given as

$$(\rho, u, p, \gamma) = \begin{cases} (0.01, 0, 1000, 2) & \text{if } 0 < x < 0.5 \\ \\ (1, 0, 1, 7.15) & \text{if } 1 > x > 0.5 \end{cases} \tag{3.3}$$

and the final time is $t = 0.008$. Case II-B is a weak impact problem, in which a gas impacts on water with very low speed. The initial condition is

$$(\rho, u, p, \gamma) = \begin{cases} (0.01, 0.01, 1, 1.4) & \text{if } 0 < x < 0.2 \\ \\ (1.0, 0, 1, 7.15) & \text{if } 1 > x > 0.2 \end{cases} \tag{3.4}$$

and the final time is $t = 0.004$.

Figure 3 gives the computed velocity, density or pressure profiles. Again, as in Case I-B, the TR and M-HLLC solvers predict a physically correct solution for Case II-B, but the original HLLC solver obtains an incorrect pressure profile and velocity profile with larger errors. It is also noted that the exact Riemann solver used for reference solutions suffers numerical difficulty for Case II-B. It fails to obtain physically correct post-shock particle velocity U_s and shock velocity D_s because the water density is almost unchanged.

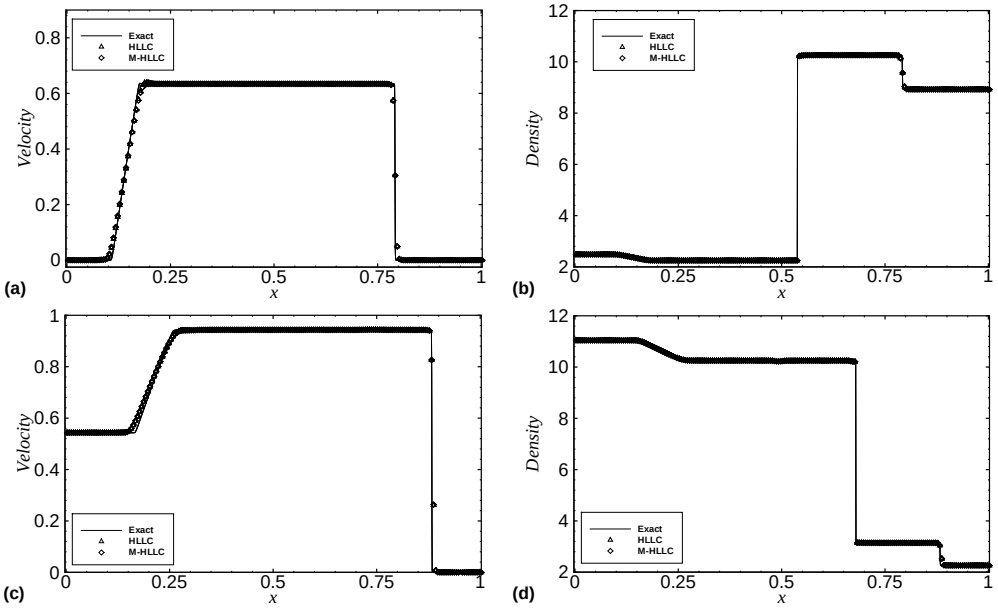

FIGURE 4. Explosion and high-speed impact: Case III-A (a) and (b); Case III-B (c) and (d).

Therefore, physically correct and accurate approximations, $U_s = 0$ and $D_s = c_0$, where c_0 is the initial sound speed of water, are given for state prediction.

3.3. *Explosive driving and high-speed impact (III)*

Two problems related to explosive driving and high-speed impact are considered next. The explosive is modeled with JWL EOS,

$$p = A_0 \exp\left(\frac{-R_1\rho_o}{\rho}\right)\left(1 - \frac{\rho}{R_1\rho_0}\right) + B_0 \exp\left(\frac{-R_2\rho_o}{\rho}\right)\left(1 - \frac{\rho}{R_2\rho_0}\right) + \Gamma_0\rho\,(e + e_0)\,,$$

where A_0, B_0, R_1, R_2, ρ_0, e_0 and Γ_0 are constant coefficients. The impacting materials are modeled by Mie-Grüneisen EOS,

$$p(\rho, e) = p_{ref} + \Gamma(\rho)\rho(e - e_{ref}),$$

where $p_{ref} = \rho_0 c_0^2\eta/(1 - s\eta)^2$, $\eta = 1 - \rho_0/\rho$, $\Gamma(\rho) = \Gamma_0\rho_0/\rho$ and $e_{ref} = 0.5p_{ref}\eta/\rho_0$. Here ρ_0, c_0, s, Γ_0 are constant coefficients. These EOSs are special cases of the general EOS given by Eq. (2.4). Because the TR solver is complicated for these types of EOS, it is not used. For similar reason, the "exact" reference solution is computed with high-resolution results on 1600 points. Case III-A, which is taken from Shyue (2001), involves the interaction between the detonation products of TNT explosive with a copper plate. The EOS coefficients of the detonation products and the copper plate are $(\Gamma, \rho_0, A_0, B_0, R_1, R_2, e_0) = (0.25, 1.84, 854.5, 20.5, 4.6, 1.35, 8.15)$ and $(\Gamma_0, \rho_0, c_0, s) = (1.96, 8.924, 3.91, 1.51)$, respectively. Here the non-dimensional references are 1000 kg/m^3 and 1 GPa. The initial condition is

$$(\rho, u, p) = \begin{cases} (2.48537, 0.0, 37) & \text{if } 0 < x < 0.5 \\ \\ (8.924, 0, 0) & \text{if } 1 > x > 0.5 \end{cases} \tag{3.5}$$

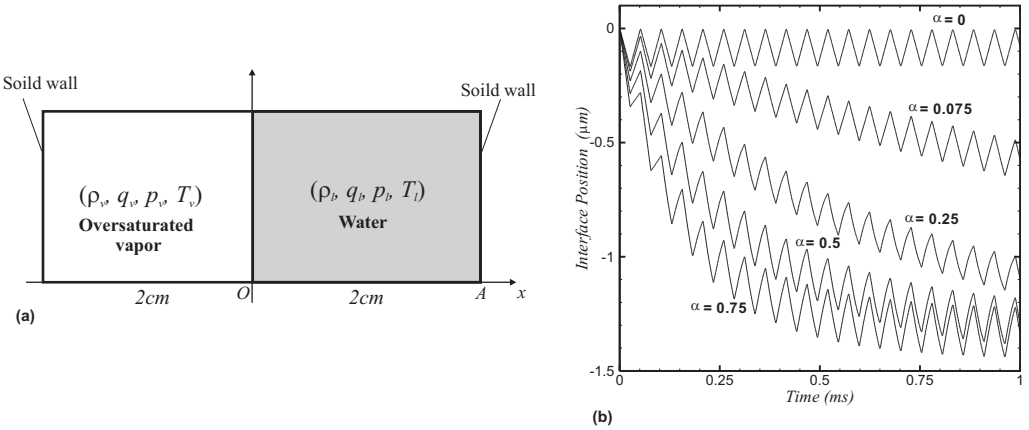

FIGURE 5. Vapor-water interaction: (a) computational domain; (b) evolution of the phase interface with different α.

and the final time is $t = 0.06$. Case III-B, which is taken from Shyue (2001), is a model shock-contact problem that involves the interaction of a shock wave in molybdenum and an encapsulated MORB (Mid-Ocean Ridge Basalt) liquid. The EOS coefficients of molybdenum and MORB are $(\Gamma_0, \rho_0, c_0, s) = (2.56, 9.961, 4.77, 1.43)$ and $(\Gamma_0, \rho_0, c_0, s) = (1.18, 2.66, 2.1, 1.68)$, respectively. The initial condition is

$$(\rho, u, p) = \begin{cases} (11.042, 0.543, 30) & \text{if } 0 < x < 0.6 \\ \\ (2.66, 0, 0) & \text{if } 1 > x > 0.6 \end{cases} \tag{3.6}$$

and the final time is $t = 0.12$.

Figure 4 gives the computed velocity, density profiles. Good agreement can be observed between the numerical and exact solutions. There is no notable difference between the results of the original and the present HLLC solvers. Note that the present methods obtain results with considerably better accuracy than those in Shyue (2001), especially for the smooth-solution regions.

3.4. *Vapor-water interaction (IV)*

We consider next problems related to vapor-water interaction. As in Case-II, the vapor is modeled with ideal-gas EOS and water is modeled with Tait's EOS. The test problem is the condensation of over-saturated water vapor in the presence of an acoustic wave. Initially, as shown in Fig. 5(a) both phases have a length of 2 cm. Vapor is on the left side and water on the right side, with the phase interface at the origin. Both phases are at rest and have a common temperature of 293 K at the beginning. The initial vapor pressure is 93 mbar, whose saturation temperature is 343 K. The water pressure is 193 mbar. The ends of the domain are reflection boundaries.

Figure 5(b) gives the evolution of the phase interface with different accommodation coefficients: $\alpha = 0$, 0.075, 0.25, 0.5 and 0.75. One can find that if there is no phase change ($\alpha = 0$), the water first expands due to its higher pressure and then shrinks and expands periodically as the pressure wave propagates back and forth in the liquid. When the phase change is included in the process, the liquid volume still oscillates, but the oscillation is superposed upon an expansion due to condensation as the vapor is over-saturated. Figure 5(b) also gives the dependence of the evolution of the interface on the accommodation

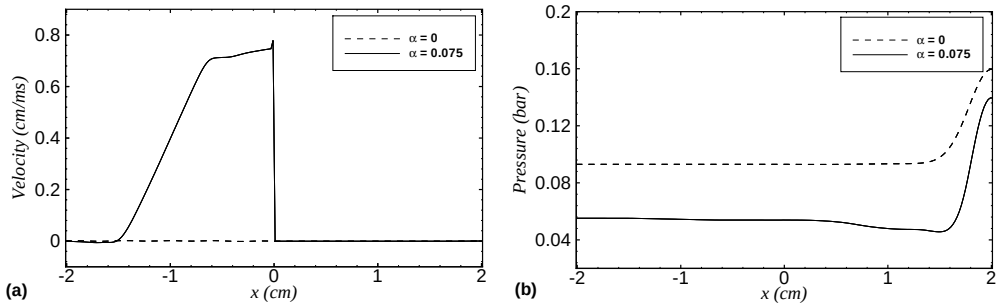

FIGURE 6. Vapor-water interaction: velocity (a) and pressure (b) profiles at $t = 1$ ms for with and without phase change.

coefficient. It can be noticed that for large α the expansion slows down due to the faster consuming of the over-saturated vapor.

Figure 6 plots the velocity and pressure profiles at 1 ms. One can find that the discontinuity of velocity in the center gives the mass flux across the phase interface (see Fig. 6(a)). With phase change considered, as the consuming of the over-saturated vapor, the pressure of both vapor and water decrease considerably (see Fig. 6(b)). These observations suggest that phase change plays an important role when deviation from phase equilibrium is present.

4. Conclusions

We have developed two extensions of our previous work on the simulation of full-Mach-range cavitating flow with sharp interface model. Specifically, we provide a new interface-interaction solver which includes a new HLLC Riemann solver and a simple phase-change model. A number of numerical examples in one dimension are studied. The obtained results suggest that the present method exhibits good robustness and accuracy. Further studies will be focused on multi-dimensional tests and possible extensions for the nucleation process.

REFERENCES

BATTEN, P., CLARKE, N., LAMBERT, C. & CAUSON D. M. 1997 On the choice of wavespeeds for the HLLC Riemann solver. *SIAM J. Sci. Comput.* **18**, 1553–1570.

BORGES, R., CARMONA, M., COSTA, B. & DON, W. S. 2008 An improved weighted essentially non-oscillatory scheme for hyperbolic conservation laws. *J. Comput. Phys.* **227**, 3191–3211.

BRENEN, C. E. 1995 *Cavitation and bubble dynamics*. Oxford University Press.

EINFELDT, B., MUNZ, C. D., ROE, P. L. & SJÖGREEN, B. 1991 On Godunov-type methods near low densities. *J. Comput. Phys.* **92**, 273–295.

FEDKIW, R., ASLAM, T., MERRIMAN, B. & OSHER, S. 1999 A non-oscillatory Eulerian approch to interfaces in multimaterial flows (the ghost fluid method). *J. Comput. Phys.* **152**, 457–492.

FUJIKAWA, S. & AKAMATSU, T. 1980 Effects of the non-equilibrium condensation of vapour on the pressure wave produced by the collapse of a bubble in a liquid. *J. Fluid Mech.* **97**, 481–512.

Guillard, H. & Murrone A. 2004 On the behavior of upwind schemes in the low Mach number limit: II. Godunov type schemes. *Comput. Fluids* **33**, 655–675.

Harten, A., Lax, P. D. & van Leer, B. 1983 On upstream differencing and Godunov-type schemes for hyperbolic conservation laws. *SIAM Rev.* **25**, 35–61.

Hu, X. Y. & Khoo, B. C. 2004 An interface interaction method for compressible multifluids. *J. Comput. Phys.* **198**, 35–64.

Hu, X. Y., Khoo B. C., Adams N. A. & Huang, F. L. 2006 A conservative interface method for compressible flows. *J. Comput. Phys.* **219**, 553–578.

Hu, X. Y., Adams N. A. & Iaccarino G. 2008 On the HLLC solver for interface interaction in compressible multi-fluid flow. *in preparation*.

Jiang, G. S. & Shu, C. W. 1996 Efficient implementation of weighted ENO schemes. *J. Comput. Phys.* **126**, 202–228.

Scharge, R. W. 1953 *A Theoretical Study of Interphme Mass Tramfer*. Columbia University Press.

Shu, C. W. & Osher, S. 1988 Efficient implementation of essentially non-oscillatory shock-capturing schemes. *J. Comput. Phys.* **77**, 439–471.

Shyue, K. M. 2001 A fluid-mixture type algorithm for compressible multicomponent flow with Mie-Gruneisen equation of state. *J. Comput. Phys.* **171**, 678–707.